Growth and Aggregation Rates for Calcite and Calcium Oxalate Monohydrate

Alan P. Collier and Michael J. Hounslow
Dept. of Chemical and Process Engineering, University of Sheffield, Sheffield, S1 3JD, U.K.

Seeded batch experiments were conducted at low magma densities and moderate ionic strength to determine the growth and aggregation rate constants for calcite precipitation in a stirred vessel. The growth was found to be surface-reaction-limited, and the growth rates agreed broadly with other studies of calcite precipitation. Aggregation rates have rarely been presented for calcite. The aggregation rate constant studied here was directly proportional to the instantaneous growth rate and inversely proportional to the average shear rate in the vessel. The results were also compared with similar work carried out on calcium oxalate monohydrate. It was found that the relationship between the aggregation rate constant and stirrer speed was virtually identical in the two cases, despite almost an order of magnitude difference in the growth rate constants.

Introduction

During precipitation from solution, several phenomena may occur. These may be classified as nucleation, growth, aggregation, and breakage. In a seeded batch system, where seed crystals are added to a metastable solution, very little nucleation takes place. In many cases, such as the study presented here, particularly where crystal growth is taking place, it can be shown that the breakage rate is negligible. Thus, aggregation and growth are often the only phenomena which alter the amount of solid material present, or the particle-size distribution (PSD). For circumstances such as these, Bramely, Hounslow, and Ryall (1996) presented a method by which the growth and aggregation rates can be extracted from experimentally measured PSDs as a function of time. If the solution composition is known or can be calculated, the growth rate can be correlated with the supersaturation, and the growth rate constant determined.

Since there is a large number of possible aggregation mechanisms, it is desirable to determine the one which is active in the case under study. Other authors, such as Hostomsky and Jones (1991, 1993), have demonstrated that the aggregation of calcite is size-independent. In this article we give an analysis of several possible aggregation kernels, and determine which best fits the experimental data obtained. The growth and aggregation rate constants may then be correlated. Aggregation rate constants were determined at a number of different agitation rates, and the relationship between the stirrer speed and the aggregation rate constant was also examined.

Many articles have been published giving growth rates for calcite, and several of these will be reviewed later in this article and compared with the results presented here. In contrast, there has been relatively little research into the aggregation of calcite, although the most important articles will again be reviewed in the light of the work reported here.

Theory

Growth

When ionic crystals grow, dispersed ions diffuse through the solution to the surface, and react to form solid material. It is possible for either the diffusion or the surface reaction to be the rate limiting stage in the process. However, if the crystals are sparingly soluble, quite small ($< 20\ \mu$m), or are in a well-mixed suspension, the diffusion of material to the surface will be rapid, and the surface reaction is likely to be the rate limiting step. In the current work, all of the above conditions are true, so it can be assumed that the crystal growth is limited by the surface reaction.

A wide range of possible surface growth mechanisms have been postulated, of which surface adsorption, spiral growth, and surface nucleation are most commonly proposed as controlling mechanisms. Expressions for the growth rate as a function of the solution properties may be derived for each

Correspondence concerning this article should be addressed to M. J. Hounslow.

of these theories, respectively. Nielsen (1984) quotes the following results

$$G = k_1(S-1) \tag{1}$$

$$G = k_2(S-1)^2 \tag{2}$$

$$G = k_3 S^{7/6}(S-1)^{2/3}(\ln S)^{1/6}\exp[-K/\ln S] \tag{3}$$

G is the growth rate ($m \cdot s^{-1}$), which is defined as the rate of change dL/dt of a typical dimension L of a crystal or group of crystals. k_i are the growth rate constants ($m \cdot s^{-1}$), which only depend on the solution temperature, and S is the relative supersaturation of the solution. For calcite, S is given by

$$S = \left(\frac{a_{Ca^{2+}} \cdot a_{co_3^{2-}}}{K_{SP}}\right)^{1/2} \tag{4}$$

where K_{SP} is the thermodynamic solubility product for calcite ($mol^2 \cdot L^{-2}$). Nancollas the Reddy (1971) quote other authors and give their own results to conclude that K_{SP} for calcite has a value of 4.7×10^{-9} $mol^2 \cdot L^{-2}$ at 25°C. This value has been used in the work presented here.

A number of articles have been published which conclude that the spiral growth mechanism described by Eq. 2 best fits the measurements of the growth of calcite from solution. The equation was derived by Burton, Cabrera, and Frank (1951) for spiral growth at screw dislocations under relatively low supersaturation conditions. Growth at spiral or screw dislocations is commonly known as the BCF growth mechanism, after the authors of the article. Recently, atomic force microscopy has been used to image the surfaces of growing calcite crystals at lattice resolution or better. Gratz, Hillner, and Hansma (1993) and Kipp et al. (1994) among others have produced clear images of growth spirals on the surface of calcite crystals growth in slightly supersaturated solutions. Therefore, it is highly likely that the spiral growth mechanism is active in this case.

Aggregation

The aggregation rate is often expressed as a kernel $\beta(L, \lambda)$ ($m^3 \cdot s^{-1}$). This kernel expresses the rate constant for successful collisions between the particles of sizes λ and L. It is now common to view this kernel as the product of two factors, that is, $\beta(L, \lambda) = \beta_0 \times f(L, \lambda)$. β_0 is not dependent on the size of the colliding particles, and is a function of the operating conditions such as the solution composition and the local fluid velocity. The factor $f(L, \lambda)$ determines the size-dependence of the aggregation reaction, and thus may include terms which have been derived from consideration of the physical processes occurring during aggregation. Many kernels have been devised either from mechanistic considerations or for reasons of mathematical ease. In the Results section, the experimental data from this work will be examined to ascertain which of the most common kernels best describes the observed aggregation in calcite.

Supersaturation

There are several problems with the calculation of the supersaturation as given by Eq. 4. Aqueous systems containing Ca^{2+} and CO_3^{2-} ions also contain a number of other ions and complexes, most notably HCO_3^- and $CaHCO_3^+$, the concentrations of which are governed by a number of equilibria. The main ones are given in Eqs. 5–9.

$$\left.\begin{array}{ll} H^+ + CO_3^{2-} \rightleftarrows HCO_3^- & K_a = 2.132 \times 10^{10} \\ Ca^{2+} + CO_3^{2-} \rightleftarrows CaCO_3(l) & K_b = 1585 \\ Ca^{2+}\,OH^- \rightleftarrows CaOH^+ & K_c = 25.12 \\ Ca^{2+}\,HCO_3^- \rightleftarrows CaHCO_3^+ & K_d = 19.4 \\ H^+ + HCO_3^- \rightleftarrows H_2CO_3(l) & K_e = 2.246 \times 10^6 \end{array}\right\} \begin{array}{l} (5) \\ (6) \\ (7) \\ (8) \\ (9) \end{array}$$

The presence of these other ions and complexes reduces the concentrations of the Ca^{2+} and CO_3^{2-} ions, altering the supersaturation. In particular, the solution pH has a large effect due to the production of HCO_3^- ions by the reaction given in Eq. 5. The supersaturation and equilibria are also defined in terms of ion activities, not concentrations. Activity coefficients must therefore be used to relate the activities to the ion concentrations. Davies' modification of the Debye-Hückel theory (Davies, 1962) was used to calculate the activity coefficients. The correlation is given in Eq. 10.

$$-\log(\gamma_{z_i,\pm})\, Az_i^2\left(\frac{\sqrt{I}}{1+\sqrt{I}}\right) + 0.3I \tag{10}$$

The activity coefficient $\gamma_{z_i \pm}$ depends on the charge z_i of the ion, but has the same value for anions and cations. The constant A has the value 0.509 for this system. I is the ionic strength ($mol \cdot L^{-1}$) and is defined by Eq. 11, where c_i is the concentration of an ionic species ($mol \cdot L^{-1}$)

$$I = \frac{1}{2}\sum_i c_i z_i^2 \tag{11}$$

Since some of the equilibria involve a change in the number of ions present, an iterative procedure was required in order to solve the series of equations for the ion concentrations, activity coefficients, and the total ionic strength.

Experimental Work

Materials and methods

The experimental protocol used in this work is a development of that described previously by Collier et al. (1996). Seed crystals of calcite were produced by nucleation from a supersaturated solution of calcium carbonate. The solution was made by dissolving calcite in acidified water, and then raising the pH by the addition of NaOH. The solution ionic strength was raised to approximately 0.15 M by the addition of KNO_3 to facilitate the use of an Elzone particle size analyzer, working on the Coulter electrical zone sensing principle.

The seed crystals were prepared as part of the procedure for each experiment; suspensions of calcite crystals were found to undergo aging with time, reducing their usefulness as seed materials. The seeds were therefore introduced to the crystallizer immediately after production to prevent unwanted changes to their form or size distribution.

The round-bottomed borosilicate glass crystallizer used in this work is shown in Figure 1. It had a nominal capacity of 1

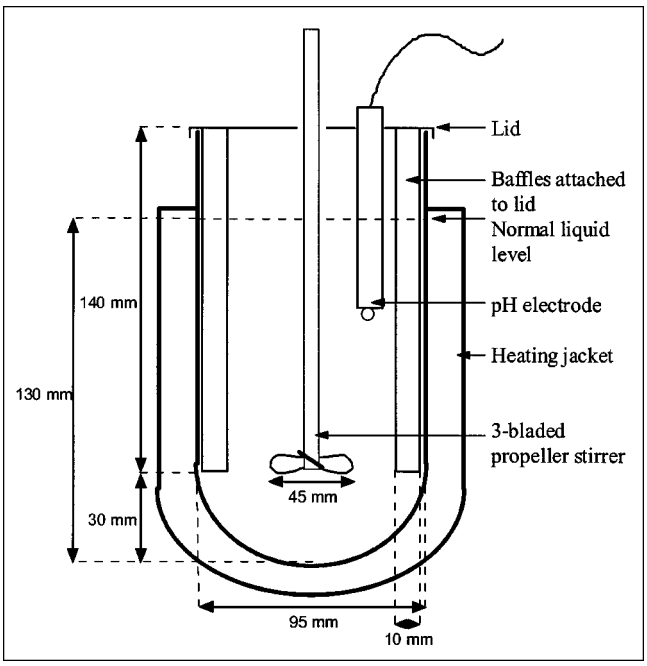

Figure 1. Jacketed crystallizer used in this work.

The four baffles and stirrer were of stainless steel. The lid was perspex, and the vessel was fabricated from borosilicate glass.

L, and was jacketed so that the experiments could be carried out at a constant temperature of 25.0 ± 0.2°C. The vessel was stirred by a 45 mm diameter, three bladed marine impeller (IKA model R1381). The central flow was directed downwards to reduce the sedimentation of the particles. A digitally controlled overhead stirrer motor (IKA model power digi-visc) was used to maintain a constant stirrer speed.

Calcium carbonate (120 mg) was dispersed in 440 mL of distilled water in a 600 mL glass beaker stirred magnetically at 600 rpm. 42 mL of 0.1-M HCl were added slowly over a period of approximately 20 s. The slow addition prevented the release of CO_2 from the solution by keeping the solution pH above 2.0. After approximately 30 s, the solution became clear, and the final pH was approximately 2.5. Once the solid had dissolved, the solution was pressure filtered through a Whatman 0.2 μm cellulose nitrate membrane. The positive pressure method was used prevent the removal of CO_3^{2-} ions from the solution by dissociation into CO_2. After filtration, the solution was returned to the beaker and stirring was resumed. 10.5 mL of 0.5-M NaOH were added from a syringe over a period of 10–15 s during which the solution pH rose to approximately 11.5. The solution was stirred continuously until nucleation occurred, which was indicated by the appearance of a white precipitate, usually after 4–5 min. The seeds were allowed to grow for 2 min after the first appearance of the precipitate, during which time the mode size of the crystals increased to 3–4 μm.

Once the seeds had been prepared, the suspension was added to the crystallizer, which already contained 400 mL of 0.34-M KNO_3. This added solution had three purposes: to increase the solution ionic strength and conductivity for particle-size analysis by the Coulter method; to quench nucleation and to reduce the growth rate for convenient measurement. The stirrer was started immediately when the seeds had been added. Small samples were withdrawn at regular intervals for size analysis, and the subsequent determination of the growth and aggregation rates.

Numerical methods

During each experiment, PSDs were measured at frequent time intervals. Bramley, et al. (1996) demonstrated that it is possible to extract the growth and aggregation rates independently of each other, and also to estimate a source function for the growth of small particles into the field of view of the particle-size analyzer.

For a system undergoing only growth and aggregation, it can be shown that the growth and aggregation rate constants can be derived independently from the volume and number of crystals respectively, using Eqs. 12 and 13

$$\frac{dm_0}{dt} = \frac{1}{2}\beta_0 m_0^2 \tag{12}$$

$$\frac{dm_3}{dt} = 3Gm_2 \tag{13}$$

where m_i is the ith moment of the PSD. For more complex systems, where small particles are growing into the field of view of the particle-size analyzer, or either growth or aggregation are size-dependent, a differential form of the population balance equation must be used. Bramly et al. derive the following equations

$$\dot{m}_0 = \beta_0\Phi_0 + B_u \tag{14}$$

$$\dot{m}_3 = G\Phi_3 + B_u\overline{L}_1^3 \tag{15}$$

$$\dot{N}_1 = G\Phi_2 + \beta_0\Phi_1 + B_u \tag{16}$$

The values of $\dot{m}_0$, $\dot{m}_3$, $\dot{N}_1$, and the parameters Φ_0, Φ_1, Φ_2 and Φ_3 can all be calculated from the experimental PSDs. Equations 14–16 may then be used to calculate simultaneously G, β_0 and B_u; the growth, aggregation, and source rate constants.

Parameters investigated

Agitation Rate. The main purpose of this work was to examine the relationship between the growth and aggregation rates as a function of the agitation rate, determined by the stirrer speed. Five different stirrer speeds N of 700, 1,100, 1,400, 1,700 and 2,000 rpm were used, and several experiments were carried out at each speed apart from 2,000 rpm. All other parameters, such as the initial concentrations and the solution ionic strength, were kept constant as far as possible.

Results and Discussion

Growth rates

Since spiral growth at screw dislocation sites has been observed directly on calcite surfaces, it is sensible to fit the observed data to Eq. 2, derived by Burton et al. (1951). Figure 2

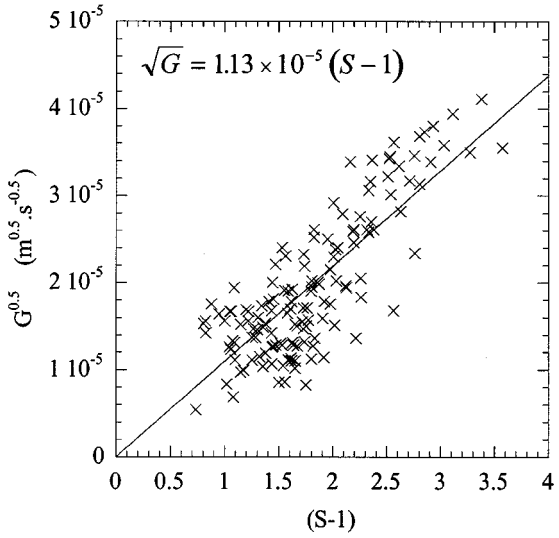

Figure 2. Plot of $\sqrt{G}$ v $(S-1)$.

This plot contains 140 data points from approximately 30 separate experiments.

shows $\sqrt{G}$ plotted against $(S-1)$ with data from all of the experiments in this study. This particular form is used since it allows easier identification of systematic errors. There is no observable difference between the growth rates at different stirrer speeds, so the points are not differentiated on the graph. Despite the scatter in the data, it can be seen that the trend is linear. The assumption of spiral growth according to the BCF growth mechanism is therefore likely to be valid. The best fit line is

$$\sqrt{G}\,(m^{0.5}\cdot s^{-0.5}) = (1.13 \pm 0.05) \times 10^{-5}(S-1) \quad (17)$$

In this study, G is used to mean the rate of change of the *diameter* of a particle, since the PSDs reported by the Coulter Multisizer are given in this form. Many workers also characterize the growth rate by the rate of change of the particle radius, here denoted $\dot{r}$ $(m\cdot s^{-1})$, using a growth rate coefficient denoted here as k_r $(m\cdot s^{-1})$. The overall growth rate equation can therefore be written

$$G(m\cdot s^{-1}) = (1.28 \pm 0.1) \times 10^{-10}(S-1)^2 \quad (18)$$

or

$$\dot{r}(m\cdot s^{-1}) = (6.4 \pm 0.05) \times 10^{-11}(S-1)^2 \quad (19)$$

These growth rate constant values (k_r) can be compared with other values in the literature.

In the article by Nancollas and Reddy (1971), some of the earliest data were presented on the growth of calcite. They correlated the growth rate as a function of (S^2-1) rather than $(S-1)^2$. They also calculated supersaturation in terms of concentrations rather than ionic species activities. However, the article contains enough information to be able to calculate a growth rate constant in more conventional terms as used here. This value of k_r is 4.22×10^{-11} $m\cdot s^{-1}$, which is slightly lower than the 6.4×10^{-11} $m\cdot s^{-1}$ reported from the current study.

Nielsen and Toft (1984) used a different method from that used by the other authors mentioned here. A graph of $\sqrt{\dot{r}}$ against the concentration is plotted, and the fitted line is extrapolated to intersect the negative ordinate axis. Using Eq. 2, it can be shown that the ordinate value where the line crosses the axis gives

$$\sqrt{k} = -\sqrt{\dot{r}} \quad (20)$$

Using this method and data presented in Figure 15 of Nielsen and Toft's article, a growth rate constant of $k_r = 1.67 \times 10^{-10}$ $m\cdot s^{-1}$ is obtained, which is considerably higher than any of the other values reported here. However, Nielsen and Toft present a value of $k_r = 4.6 \times 10^{-11}$ $m\cdot s^{-1}$ in Table 1 of their article. A short note in the text mentions that all data points at concentrations > 0.23 mM have been neglected in obtaining this value, with no explanation. This method is likely to be unreliable for two reasons. First, overall carbonate concentrations were used in the plot, rather than carbonate ion activities. This will cause curvature in the plot, leading to difficulty in determining the axis intercept. Secondly, it is often difficult to measure low growth rates accurately. In this case, there will be a considerable extrapolation from the reliable data to the ordinate axis, exaggerating any error in the measured slope, particularly in light of the possible curvature of the line.

Kazmierczak et al. (1982) used a constant composition method to determine the growth rate constant at a number of solution ionic strengths. A slight confusion in terminology is apparent from the text. Kazmierczak et al. appear to use two different forms for the supersaturation. Δ is used as the equivalent of $(S-1)$ in this article, and values for S^b are quoted in Table 1, where S^b is equivalent to (S^2-1) in this article. If the values for S^b are used to calculate S, the growth rate constant can again be determined. In this case a value of $k_r = 4.97 \times 10^{-11}$ $m\cdot s^{-1}$ is obtained.

More recently, Tai et al. (1993) reported results from an analysis which did not assume that the growth was second order. Growth rates were also calculated separately for particles of different sizes. It should be noted that the authors used a value for the solubility product of calcite (K_{SP}) of 1.42×10^{-8} rather than 4.7×10^{-9} $mol^2\cdot l^{-2}$, which is the more commonly accepted value (Nancollas and Reddy, 1971). For small (2 μm particles), Tai et al. found that the growth rate was dependent on the supersaturation to the power 2.25. For larger particles, this power was almost exactly 2, indicating that the growth probably occurs by the BCF mechanism. The growth rate constant also appeared to vary with the particle size. For 5 μm particles, the growth rate constant reported is $k_r = 3.63 \times 10^{-11}$ $m\cdot s^{-1}$. The authors reported that the growth rate was dependent on the particle size to the power 0.6. Tai et al. do not compare their analysis of the size-dependence of the growth of calcite crystals with work from any other groups.

The growth rate coefficient presented here falls within the range of values reported by other authors, although it is slightly higher than those calculated by other methods.

Aggregation rates: determining the best kernel

Aggregation is more complex to analyze than growth, since it is influenced by more experimental parameters. The results presented in this section show that, in this case, the aggregation rate is a simple function of the growth rate G and the stirrer speed N. It is also likely that the solution ionic strength also influences the aggregation rate, but this is outside the scope of the current work.

With aggregation, as with growth, it is desirable to identify the operative mechanism. In the current work, this is done by finding the kernel that best describes the observed aggregation rates. It is now possible to perform numerical integration of the aggregation rate equation, enabling the prediction of the product PSD from an experiment. This technique can be used as a test of the suitability of an aggregation kernel. For a given experiment, the growth and aggregation rates are determined from measured PSDs using the method of Bramley et al. (1996), and the aggregation rate constant β_0 is calculated for each of the kernels under investigation. The growth and aggregation rate constants are then correlated with time or supersaturation, and, for each kernel, the population balance equation is integrated. A sum-of-squares method is then used to determine which of the kernels best predicts the observed PSD.

In this work, three kernels are tested: size-independent, Brownian motion, and shear. These kernels have been shown (Smit et al., 1995) not to be gelling kernels, and therefore they are suitable for this work, where gelation is not observed. Figures 3 and 4 show the PSDs observed during a typical experiment at 1,400 rpm, those calculated using the three kernels. The times are 40 and 80 min after the start of the experiment, respectively.

It can clearly be seen that the shear kernel is a poor model for the observed results. The other kernels are more difficult to distinguish. The sum-of-squares error calculation shows that the size-independent kernel is the best fit for the observed data, so this kernel will be used in the analysis of the results from this work. Other workers in this area (Hostomsky and Jones, 1991, 1993; Wójcik and Jones, 1997) have also found the size-independent kernel to be the one which best describes the aggregation of calcite in precipitating conditions.

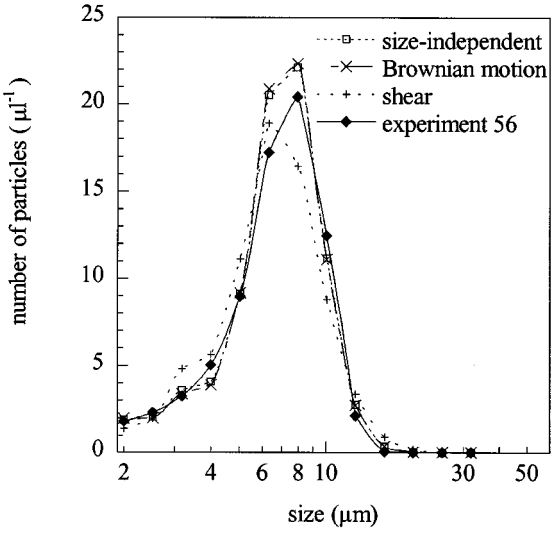

Figure 3. PSDs measured from a typical experiment at 1,400 rpm, and simulated using various kernels after 40 min.

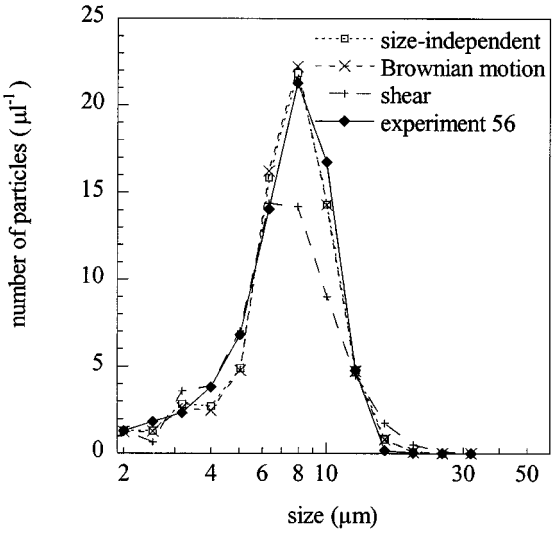

Figure 4. PSDs measured from a typical experiment at 1,400 rpm, and simulated using various kernels after 80 min.

Aggregation rates: measuring the rates

The main objective of our work was to examine the relationship between the aggregation rate constant β_0 and the agitation rate in the vessel, measured by the stirrer speed. For each particular stirrer speed, it was found that there was a roughly linear relationship between β_0 and the growth rate. As the stirrer speed was increased, the aggregation rate was found to fall. Figure 5 shows the relationship between β_0 and G as a function of stirrer speed.

Since several experiments were conducted at each stirrer speed except 2,000 rpm, it was convenient to collect the data into groups to typically eight data points. The average values for each group were then plotted in Figure 5, along with an estimate of the error. This allows the trends in the data to be seen more clearly, as well as providing the error estimate.

Lines are fitted through the origin. For all stirrer speeds except 700 rpm, it was found that lines of the form $y = f_1 \cdot x + f_2$ would pass very close to the origin. At 700 rpm, the positive aggregation rate at zero growth rate is thought to be an artefact caused by the larger particles sticking to the vessel walls, thereby altering the measured growth and aggregation rates. It is worth noting that no breakage of the particles was found during the work. Several experiments were left to run for 10–12 h instead of the normal 2 h. The breakage rate is likely to be independent of the supersaturation, so its effects should be more noticeable at long times, once aggregation has stopped due to the supersaturation being exhausted. If breakage of the particles was occurring, the number of small particles would increase, and the mode of the PSD would move to a smaller size. Neither of these effects was observed, so it is concluded that breakage occurred at a negligible rate.

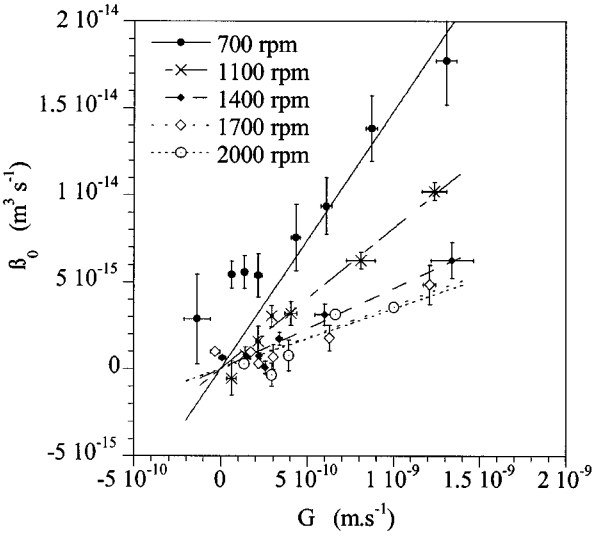

Figure 5. Combined plot of β_0 against G for all stirrer speeds examined.

The decrease in slope with increasing stirrer speed can clearly be seen.

Since the lines fitted to the β_0 against G data passed almost through the origin, lines of the form

$$\beta_0 = f \cdot G \tag{21}$$

were fitted to the data for each stirrer speed. The slopes f of these lines were then correlated with the stirrer speed. Figure 6 shows f plotted against the stirrer speed on a double logarithmic plot.

The line fitted to the data has a slope of -1.48. Once a correlation has been established, it may be useful to determine the origins of the terms found. The most obvious term to examine is the stirrer speed N. It has been suggested by

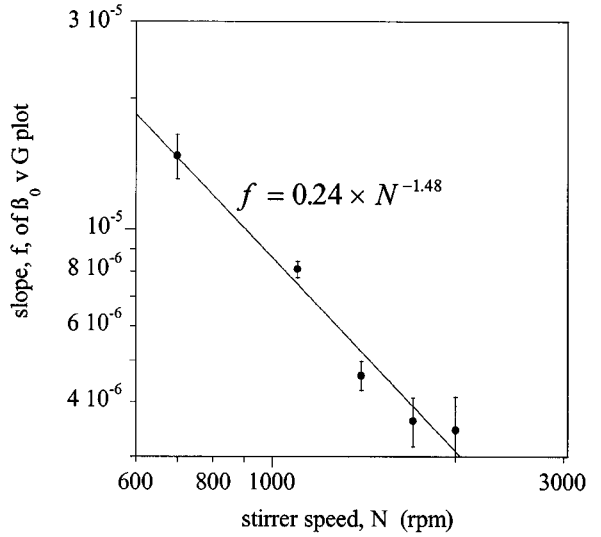

Figure 6. Plot of f against N for the 5 stirrer speeds used.

Koh, Andrews, and Uhlherr (1987) that the average shear rate $\bar{\dot{\gamma}}$ (s^{-1}) in a stirred vessel can be described by Eq. 22

$$\bar{\dot{\gamma}}\sqrt{\frac{P}{\mu V}} \tag{22}$$

The power input to a vessel if often correlated using the power number for the design of stirrer being used. The power number is defined by Eq. 23.

$$N_p = \frac{P}{\rho N^3 D^5} \tag{23}$$

where P is the total power input (W), ρ is the fluid density ($kg \cdot m^{-3}$), N is the rotation rate in revolutions per second (s^{-1}), and D is the diameter of the stirrer (m). At high stirrer Reynolds numbers, N_p is constant. In this work, $23600 < Re < 67400$. Thus, for a particular stirrer, the power input to the fluid is proportional to the cube of the stirrer speed. If Eqs. 22 and 23 are combined, it can be seen that the average shear rate is proportional to the stirrer speed to the power 1.5. If this result is compared with the slope (-1.48) of the logarithmic plot in Figure 6, it can be seen that the aggregation rate is inversely proportional to the average shear rate in the system, that is, $\beta_0 \propto 1/\bar{\dot{\gamma}}$.

Hostomsky and Jones (1991) measured aggregation rates of 4.33×10^{-14} and 3.17×10^{-14} $m^3 \cdot s^{-1}$ at stirrer speeds of 600 and 1,800 rpm. These values do not show such a strong dependence on the stirrer speed as found in this work. However, the values are also considerably higher than those reported here (1.5×10^{-14} and 3.6×10^{-16} $m^3 \cdot s^{-1}$ at 700 and 2,000 rpm, respectively). Since the aggregation rates are higher, it is also likely that the growth rates are higher than those measured in this study. Hostomsky and Jones report only an apparent growth rate, which is an order of magnitude greater than those from the current work.

In another article Hostomsky and Jones (1993) reported an aggregation rate of 1.42×10^{-13} $m^3 \cdot s^{-1}$ using the same apparatus as in their pervious work, with a stirrer speed of 1,200 rpm. This aggregation rate is much higher than those reported in the earlier article, and no explanation is offered by the authors. Work by Mumtaz et al. (1997) suggested that the aggregation rate tends to zero at very low and very high agitation rates with a maximum value in between. At low agitation rates, there are very few collisions between the suspended particles, giving a low aggregation rate. A high agitation rates, there are many collisions, but the majority do not lead to aggregation events since new aggregates are pulled apart by the large hydrodynamic forces before a stable particle has time to develop. Between these extremes, there are a reasonable number of collisions, some of which are successful, giving a moderate aggregation rate. It is possible that the results presented by Hostomsky and Jones lie around this maximum point in the curve, while the results from the current work are on the descending part of the curve.

Wójcik and Jones (1997) used an alternative analysis method to calculate simultaneously rate constants for nucleation, growth, aggregation and breakage during calcite precipitation. The growth rates quoted are an order of magnitude greater than those found during this work. However, the

authors give enough information to calculate values for the supersaturation, and the values are roughly comparable with Eq. 19. The size-independent aggregation rates presented are surprisingly small. It would be expected that an aggregation kernel calculated in the presence of a breakage kernel would be larger than a combined kernel. The values presented by Wójcik and Jones are three orders of magnitude smaller than those presented from this work. There is also little obvious difference between the aggregation kernels at the different stirrer speeds. The considerable differences between the results of Wójcik and Jones and the others considered here are almost certainly attributable to the different method used to extract the rates from the experimental data, and the use of separate breakage and aggregation kernels. In this article, we have used aggregation rate to mean the net rate of successful aggregation events. We have also determined that once the aggregates have formed, the breakage rate is negligible. The model used by Wójcik and Jones does not differentiate between unsuccessful collisions events and the breakage of firmly bound aggregates. It therefore cannot cope with the variation in strength of the crystalline bridges between the particles as the aggregation process proceeds. Wójcik and Jones find a significant breakage rate, because their method identifies a large fraction of the unsuccessful collisions as breakage events.

Comparison between calcite and calcium oxalate

Calcium oxalate is a similar system to calcite in several ways: it has a low solubility product (2.24×10^{-9} mol$^2\cdot$L^{-2} reported by Bramley et al., 1996), exhibits several polymorphs, depending on the degree of hydration of the crystals, and has been widely studied due to its importance in biological systems. Bramley et al. (1997) present a growth rate coefficient k for calcium oxalate of 1.45×10^{-9} m$\cdot$s^{-1}, which is an order of magnitude greater than that for calcite (1.28×10^{-10} m$\cdot$s^{-1}) given in Eq. 18.

Work by Barrick et al. (1998) on the calcium oxalate monohydrate (COM) system gives some information on the dependence of β_0 on N, over a limited range. The experimental equipment was identical to that used in the current work. Figure 7 shows the data from Figure 6 for the results from the current work alongside the data given by Barrick. It can be seen that only three stirrer speeds have been used in the COM study (600, 800 and 1,000 rpm). The data show a remarkable correlation with those from the current work, despite the growth rate coefficients being almost almost an order of magnitude different.

Since the data from two different systems match so well, it is hoped that this type of correlation can be used to simplify the analysis and prediction of aggregation rates from many other systems.

Conclusions

The batch precipitation of calcite has been investigated, and the growth and aggregation rate constants measured. The growth of calcite was found to be size-independent, and second-order in supersaturation, with a rate constant of $k_r = 6.4\times10^{-11}$ m$\cdot$s^{-1}. This value compares well with other published values calculated by other methods. Aggregation was also found to be size-independent. The aggregation rate constant β_0, was found to be directly proportional to the instantaneous growth rate, and inversely proportional to the volume averaged shear rate, or to the stirrer speed to the power -1.5.

The relationship between β_0 and the stirrer speed was compared with similar work on calcium oxalate monohydrate. It was found that both sets of data could be fitted to a single line, despite an order of magnitude difference in the growth rate coefficients for calcite and calcium oxalate.

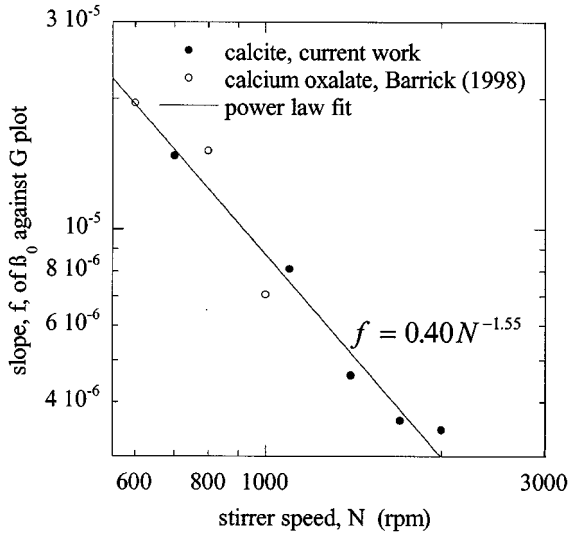

Figure 7. Plot of *f* against *N* for calcite from the current work, and from calcium oxalate monohydrate data supplied by Barrick et al. (1998).

Acknowledgment

This work was funded by the EPSRC of the United Kingdom.

Notation

a = solute activity, mol$\cdot$l^{-1}
B_u = source rate coefficient, m$^{-3}\cdot$s^{-1}
f = slope of β_0vG plot, m^2
L = particle diameter, m
m_i = moment of order i of a PSD, m$^i\cdot$m^{-3}
N_1 = rate of change of the number of particles in the first size interval of a PSD, m$^{-3}\cdot$s^{-1}
V = vessel volume, m^3
β_0 = constant part of aggregation kernel m$^3\cdot$s^{-1}
λ = particle diameter, m
μ = liquid viscosity, m$^2\cdot$s^{-1}

Acronyms

COM = calcium oxalate monohydrate

Literature Cited

Barrick, J. P., M. J. Hounslow, A. S. Bramley, and H. S. Mumtaz, ''A Study of the Aggregation during Precipitation of Calcium Oxalate Monohydrate,'' *Proc. 1998 I. Chem. E. Annual Research Event*, Newcastle, U.K. (1998).

Bramley, A. S., M. J. Hounslow, and R. L. Ryall, ''Aggregation during Precipitation from Solution: A Method for Extracting Rates from Experimental Data,'' *J. Colloid Int. Sci.*, **183**(1), 155 (1996).

Bramley, A. S., M. J. Hounslow, and R. L. Ryall, ''Aggregation during Precipitation from Solution: Kinetics for Calcium Oxalate Monohydrate,'' *Chem. Eng. Sci.*, **52**, 747 (1997).
Burton, W. K., N. Cabrera, and F. C. Frank, ''The Growth of Crystals, and the Equilibrium Structure of their Surfaces,'' *Phil. Trans. Roy. Soc. (London)*, **243**, 299 (1951).
Collier, A. P., C. J. D. Hetherington, and M. J. Hounslow, ''High Resolution Imaging of Crystalline Agglomerates,'' *Chem. Eng. Res. Des.*, **74**:**A7**, 759 (1996).
Davies, C. W., *Ion Association*, Butterworths, London, U.K., p. 38 (1962).
Gratz, A. J., P. E. Hillner, and P. K. Hansma, ''Step Dynamics and Spiral Growth on Calcite,'' *Geochimica et Cosmochimica Acta*, **57**, 491 (1993).
Hostomsky, J., and A. G. Jones, ''Calcium Carbonate Crystallisation and Form During Continuous Precipitation from Solution,'' *J. Phys. D: Appl. Phys.*, **24**, 165 (1991).
Hostomsky, J. and A. G. Jones, ''Crystallization and Agglomeration Kinetics of Calcium Carbonate and Barium Sulphate in the MSMPR Crystallizer,'' *Proc. Symp. on Industrial Crystallization*, **2**, 49 (1993).
Johrde, L. G., and F. H. Cocks, ''The Effect of pH on the Microhardness of Renal Calculi,'' *J. Biomed. Mat. Res.*, **20**, 945 (1986).
Kazmierczak, T. F., M. B. Tomson, and G. H. Nancollas, ''Crystal Growth of Calcium Carbonate—a Controlled Composition Study,'' *J. Phys. Chem.*, **86**, 103 (1982).
Kipp, S., S. Kammer, R. Lacmann, J. Rolfs, U. Tanneburger, and W. Beckmann, ''Imaging Crystal-Growth Features Using Scanning Force Microscopy (SFM),'' *Crystal Res. and Technology*, **29**, 1005 (1994).
Koh, P. T. L., J. R. G. Andrews, and P. H. T. Uhlherr, ''Modelling Shear-Flocculation by Population Balances,'' *Chem. Eng. Sci.*, **42**, 353 (1987).
Mumtaz, H. S., M. J. Hounslow, N. A. Seaton, and W. R. Paterson, ''Orthokinetic Aggregation During Precipitation: A Computational Model for Calcium Oxalate Monohydrate,'' *Chem. Eng. Res. Des.*, **75**:**A2**, 152 (1997).
Nancollas, G. H., and M. M. Reddy, ''The Crystallization of Calcium Carbonate: II. Calcite Growth Mechanism,'' *J. Coll. Int. Sci.*, **37**, 824 (1971).
Nielsen, A. E., ''Electrolyte Crystal Growth Mechanisms,'' *J. Crystal Growth*, **67**, 289 (1984).
Nielsen, A. E., and J. M. Toft, ''Electrolyte Crystal Growth Kinetics,'' *J. Crystal Growth*, **67**, 278 (1984).
Smit, D. J., M. J. Hounslow, and W. R. Paterson, ''Aggregation and Gelation III: Numerical Classification of Kernels and Case Studies of Aggregation and Growth,'' *Chem. Eng. Sci.*, **50**, 849 (1995).
Tai, C. Y., P.-C. Chen, and S.-M. Shih, ''Size-Dependent Growth and Contact Nucleation of Calcite Crystals,'' *A. I. Chem. E. J.*, **39**, 1472 (1993).
Wójcik, J. A., and A. G. Jones, ''Experimental Investigation into Dynamics and Stability of Continuous MSMPR Agglomerative Precipitation of $CaCO_3$ Crystal,'' *Chem. Eng. Res. Des.*, **75**:**A2**, 113 (1997).

Manuscript received Feb. 10, 1999, and revision received July 12, 1999.